Spatial evolution of the ferromagnetic phase transition in an exchange graded film

B. J. Kirby,[1,*] H. F. Belliveau,[2] D. D. Belyea,[2] P. A. Kienzle,[1]
A. J. Grutter,[1] P. Riego,[3] A. Berger,[3,†] and Casey W. Miller[4,‡]

[1] *Center for Neutron Research, NIST, Gaithersburg, MD 20899, USA*
[2] *Department of Physics, University of South Florida, Tampa, FL 33620*
[3] *CIC nanoGUNE Consolider, E-20018 Donostia - San Sebastian, Spain*
[4] *School of Chemistry and Materials Science, Rochester Institute of Technology, Rochester, NY, 14623*

(Dated: April 7, 2015)

A combination of experiments and numerical modeling was used to study the spacial evolution of the ferromagnetic phase transition in a thin film engineered to have a smooth gradient in exchange strength, and thus effectively a gradient in local transition temperature. For a Ni_xCu_{1-x} alloy film with depth-dependent Ni concentration, we observe that the entirety of the sample is magnetically ordered at low temperatures, and that a mobile boundary separating ordered and disordered regions emerges as temperature is increased. We demonstrate continuous control of the boundary position with temperature, and control of the magnetically ordered sample volume with magnetic field. This functionality is observed near room temperature, and may enable a variety of novel thermomagnetic applications.

INTRODUCTION

The precise fabrication of magnetic heterostructures can lead to control of the physical properties of the system, including magnetic ordering. Ramos et al.[1], for example, showed that heterostructures composed of distinct antiferromagnetic materials with independent order parameters can be made to effectively exhibit a single phase transition at intermediate temperatures; Wang and Mills provided a theoretical treatment for such systems.[2] Along the same lines, Marcellini et al., used finite size effects to study the novel magnetic ordering of Fe/V multilayers in which each layer had distinct ordering temperatures.[3] Complementing these more traditional heterostructures, recent work has aimed to develop materials with functionality that arises from physical properties that are tuned by smoothly changing the growth conditions or film composition. A poignant example applicable to next generation magnetic recording focused on magnetic switching in films that contain a magnetic anisotropy gradient along its thickness.[4–8] Recently, Le Graët et al., demonstrated the ability to move an antiferromagnet-ferromagnet phase boundary with temperature by introducing a gradient of dopants into the FeRh system.[9]

In this letter we consider the nature of the ferromagnetic phase transition in a thin film with a smooth gradient in the local exchange strength J. Within a mean field framework, J is proportional to Curie temperature, T_C,[10] allowing the exchange gradient to be loosely thought of as a distribution of local T_C. The nickel-copper system was chosen because it forms isomorphous solid solutions with T_C that changes linearly with composition.[11, 12] Thus, by varying the nickel content in real-time during growth, we can form $Ni_{x(z)}Cu_{1-x(z)}$ films with a pronounced depth dependence in the local magnetic environment. We used polarized neutron reflectometry (PNR) to determine the temperature and field dependent magnetization depth profiles, and developed a model of the structure within a mean field framework in order to fit the PNR data. Our results indicate the ability to control the displacement of a quasi phase boundary between effectively ferromagnetic and effectively paramagnetic regions in graded films, which may have implications for a variety of thermomagnetic or spin caloritronic applications.

SAMPLE PREPARATION

100 nm thick (111) textured $Ni_{x(z)}Cu_{1-x(z)}$ alloy films capped with 5 nm of Ta were deposited on Si substrates. The graded sample composition varied linearly from $x = 0.61$ at the substrate interface to 0.70 at the top of the film (depicted in the Fig. 1 inset). Uniform control samples with $x = 0.61$ and $x = 0.70$ corresponding to the minimum and maximum compositions were also grown. Figure 1 shows the derivative of the magnetic moment with respect to temperature (T) for each of the three samples, as measured in a 60 mT field with vibrating sample magnetometry (VSM). The T-dependent derivatives for the uniform samples exhibit distinct minima at 202 K and 296 K, indicative of the respective Curie temperatures. These values of T_C were used to approximate the values of x. The corresponding peak in the data for the graded sample falls in between those of the uniform samples. The feature is significantly broader for the graded film, suggesting that the magnetic ordering takes place over a broad temperature range. Given the intentionally engineered composition gradient, this smearing suggests that the ferromagnetically ordered fraction of the film shrinks in volume with increasing temperature, with that change propagating from the low toward the high Ni-content region. Thus, it is interesting to consider

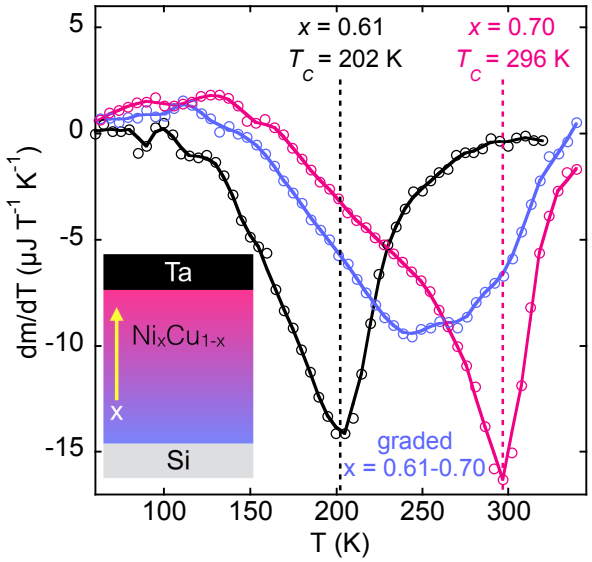

FIG. 1. Derivative of magnetic moment with respect to temperature for the uniform $x = 0.61$ (black), graded $x = 0.61$ – 0.70 (purple), and uniform $x = 0.70$ (pink) Ni_xCu_{1-x} samples, as measured in a 60 mT field. Curie temperatures for the uniform x samples are indicated by dashed vertical lines. Inset shows schematic of the graded sample.

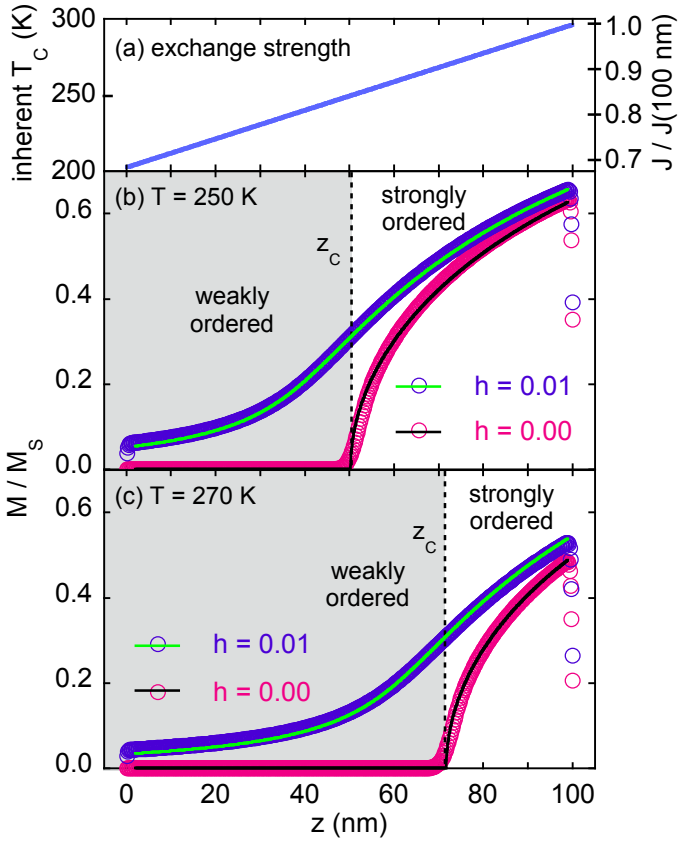

FIG. 2. Exchange strength gradient model. (a) Depth dependent exchange strength in terms of inherent T_C. (b-c) Magnetization profiles at 250 K and 270 K, respectively. Symbols in (b-c) are the results of mean-field simulations, solid lines are fits to mean-field results using a closed-form function. Dashed vertical lines in (b-c) indicate z_C, the boundary between the weakly (shaded) and strongly ordered regions.

the boundary between the magnetically ordered and disordered regions, and how that boundary moves through the structure in response to temperature and magnetic field.

EXCHANGE STRENGTH GRADIENT MODEL

The temperature and field dependent magnetic depth profile of the graded Ni_xCu_{1-x} film was treated theoretically via mean-field simulations of an exchange strength gradient model. 500 layers of ferromagnetically coupled spins were arranged on a fcc(111) lattice with 0.2 nm lattice spacing. To account for the x gradient, J is increased linearly with distance from the bottom interface (z), in accord with the inherent T_C corresponding to the local stoichiometry. For the simulations, the inherent T_C was varied from 202 K - 296 K.[13] Effects of applied magnetic field were accounted for in terms of an additional Zeeman energy term proportional to the applied field h, described in units of the local exchange field at $T = 0$ K.

Figure 2 shows the results of the simulation (open symbols) in both zero ($h = 0.00$) and nonzero ($h = 0.01$) applied field for (b) 250 K and (c) 270 K. Fig. 2 (b) shows that for a graded exchange strength, as the true T_C is approached in zero field (lower curve), the sample divides into strongly and weakly (effectively zero) magnetized regions, separated by a boundary at a "critical depth", z_C. As the applied field is increased to $h = 0.01$ (upper curve, Fig. 2(b)), the magnetization increases everywhere, but particularly so near z_C. As such, the boundary at z_C can be thought of as separating a strongly magnetized region analogous to a typical ferromagnet from a weakly magnetized region that exhibits a more paramagnetic character. Fig. 2(c) shows that z_C increases significantly for a 20 K temperature change, sliding closer to the high J end of the structure. Thus, the simulation predicts that a sufficient gradient in J should result in an quasi phase boundary that can be moved continuously along the vertical axis with temperature, and significantly modified with applied field. It is noteworthy that this quasi phase front and its motion along the growth axis should not be hysteretic because it is associated with a second order phase transition, and thus no metastable states exist.

We derived a closed-form function that closely mimics the T and h dependent profiles determined from the mean-field simulations for model fitting the PNR data.[14] The function is parameterized in terms of the slope of the exchange strength, $A = dJ/dz$, z_C, and h.

Best-fits of this functional form to the simulated profiles are shown as solid lines in Fig. 2. The fits correspond to values of h and A that match the input values of the mean-field simulation, and self-consistent fitted values of z_C. The agreement between the closed-form function and the mean-field simulation is excellent, demonstrating that the closed form function is suitable for modeling the data.

PNR MEASUREMENTS

To confirm that the graded film exhibits the anticipated behavior, polarized neutron reflectometry was used to determine the temperature and applied magnetic field (H) dependent magnetization depth profiles of the $Ni_{x(z)}Cu_{1-x(z)}$ sample. Measurements were taken over a range of temperatures in in-plane fields of either 5 mT or 500 mT. PNR is sensitive to the compositional and in-plane magnetization depth profiles of thin films and multilayers,[15] and is an invaluable tool for characterization of magnetic proximity effects in multilayers.[16, 17] Depth profiles of the nuclear scattering length density ρ_N (related to the nuclear composition) and the component of the sample magnetization (M) parallel to H can be determined by model fitting of the non spin-flip reflectivities R^{++} (incident and scattered neutron moment parallel to H) and R^{--} (antiparallel to H).

The measurements show that the $Ni_{x(z)}Cu_{1-x(z)}$ film indeed separates into strongly and weakly magnetized regions, confirming the mean-field prediction. This behavior can be illustrated by considering three characteristic conditions:

- I: 500 mT, 145 K,
  $T < T_C(x = 0.61) < T_C(x = 0.70)$,
  high field, below all inherent T_C
- II: 500 mT, 275 K,
  $T_C(x = 0.61) < T < T_C(x = 0.70)$,
  high field, between min and max inherent T_C
- III: 5 mT, 275 K,
  $T_C(x = 0.61) < T < T_C(x = 0.70)$,
  low field, between min and max inherent T_C

The fitted reflectivities for conditions I-III show clear spin-dependent oscillations, indicating sensitivity to the nuclear and magnetic depth profiles (Fig. 3(a)). Splitting between R^{++} and R^{--} arises from the component of M parallel to H.[15] Thus, to highlight the magnetic contribution to the scattering, the fitted reflectivities are plotted in Fig. 3(b) as spin asymmetry (the difference in R^{++} and R^{--} divided by their sum). All three states show distinct spin asymmetries, indicating appreciable changes to the magnetic depth profile driven by T and H.

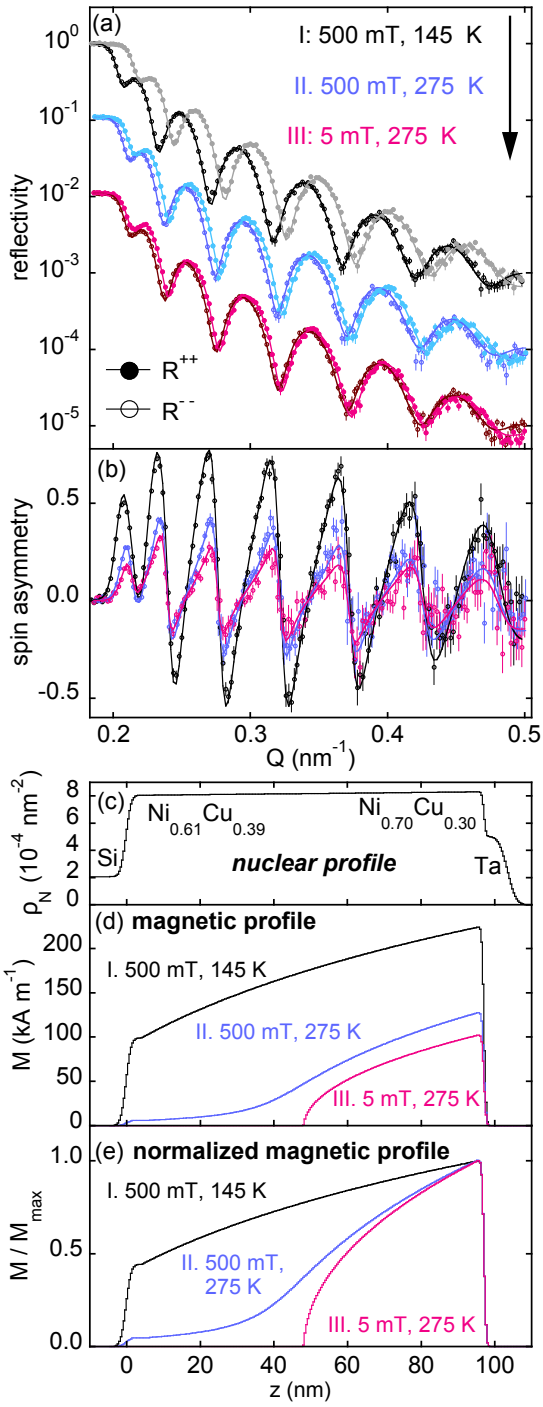

FIG. 3. (a) Fitted reflectivities for conditions I-III described in the text (vertically offset for clarity). (b) Spin asymmetries corresponding to the fitted reflectivities in (a). (c) Nuclear profile used to fit data at all H and T. (d) Magnetization depth profiles determined from the fits in (a). (e) Profiles in (d) normalized by respective maximum values.

TABLE I. Best-fit parameters associated with the magnetic profiles in Fig. 3(d). The parameter range corresponding to ±2 standard deviations in fitting uncertainty is shown in square brackets (note that the range is asymmetric).

state	z_C (nm)	h ($\times 10^{-3}$)	M_{max} (kA m^{-1})
I	-15 [-26, -9]	6 [4, 10]	224 [215, 228]
II	44 [43, 50]	6 [4, 10]	127 [124, 134]
III	44 [43, 50]	0 [0, 2]	102 [99, 106]

The fits to the data are excellent, and correspond to the nuclear and magnetic depth profiles shown in Fig. 3(c) and (d), respectively. The nuclear profile used for all conditions (Fig. 3(c)) consists of a Si substrate, a linearly graded $Ni_{x(z)}Cu_{1-x(z)}$ film, and Ta cap layer. The magnetic profile is parameterized in terms of the aforementioned closed-form function with free parameters z_C and h, convoluted with a sloped line to account for the x-dependent variation in total moment. An additional parameter corresponding to the peak magnetization of the profile, M_{max}, was used as a scaling factor. As in our mean-field simulations, z_C is assumed to be field-independent, and h is assumed to be temperature-independent. This is a tightly constrained model based on a thermodynamic mean-field simulation of the system that we believe provides the most insight into the underlying physics. Simpler models lacking the primary features of the exchange strength gradient model (e.g., a uniformly magnetized Ni_xCu_{1-x} layer) do not fit the data, and can be explicitly dismissed as potential solutions.[18]

The best-fit magnetic profiles for conditions I-III are shown in Fig. 3(d); specific parameters are listed in Table 1. For condition I, z_C is negative, indicating that the entire sample is strongly magnetized. At condition II, z_C jumps to +43 nm, indicating the sample has divided into weakly and strongly magnetized layers. This separation is made more apparent by normalizing the profiles by M_{max} as shown in Fig. 3(e). For condition III, the fitted value of h drops to zero, corresponding to the profile magnetization dropping to zero for $z < z_C$. Thus, at 275 K, the $Ni_{x(z)}Cu_{1-x(z)}$ film is in a quasi phase separated state, as predicted by the mean-field simulations (Fig. 2). Repeated cycling of the field between 5 mT and 500 mT at 275 K does not impact the PNR spectra, which demonstrates the expected lack of hysteresis in the system.[19]

Figure 4(a-c) shows the magnetic profiles at 293 K, 275 K, and 255 K, and reveals continuous, monotonic motion of z_C with changing T, along with a strong H dependencies, particularly for the effectively paramagnetic region. Figure 4(d) and (e) show the evolution of the integrated profile magnetization divided by the $Ni_{x(z)}Cu_{1-x(z)}$ film thickness (i.e. the net magnetization) and the critical depth z_C, respectively, over the entire range of temperatures studied. The strongly field

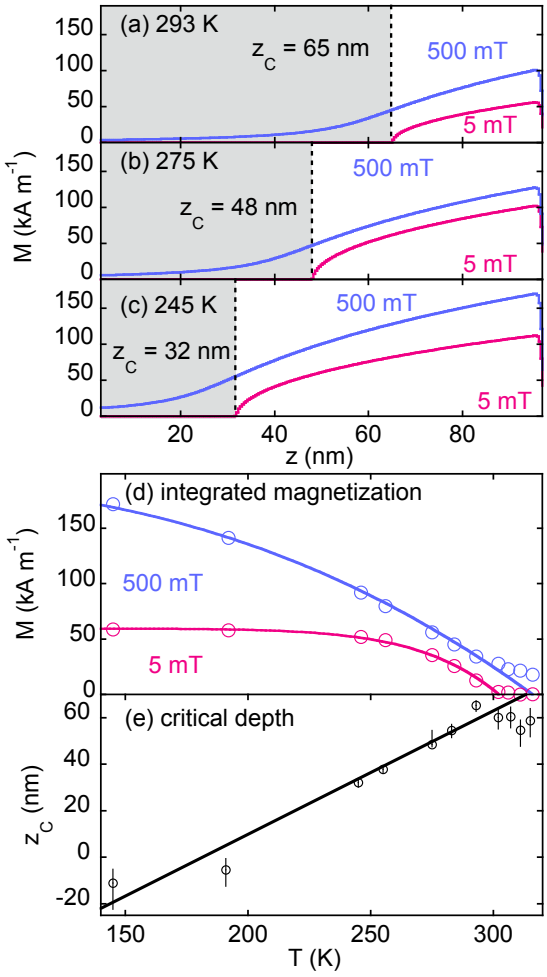

FIG. 4. (a-c) Experimentally determined magnetization profiles at selected temperatures. $z_C(T)$ is indicated by dashed vertical lines, with shading indicating the weakly ordered region. (d) Temperature-dependent depth-integrated magnetizations. (e) Temperature dependence of z_C. Error bars correspond to ±2 standard deviations, solid lines in (d-e) are guides to the eye.

dependent net magnetization approaches zero near the inherent T_C of the high x end of the sample (292 K), with a critical depth that moves monotonically towards the high x end with increasing T. The integrated magnetizations show good agreement with VSM and SQUID magnetometry, a strong validation of the model used to fit the PNR data.[20]

DISCUSSION

This work demonstrates continuous control of the displacement of a phase boundary between weakly and strongly magnetically ordered regions in a thin film structure, with functionality at and around room temperature. The extension to systems with technological relevance for

magnetic recording, such as FePt, is obvious. Since the exchange length in these high anisotropy systems is only a few nanometers, it should be possible to engineer 10-20 nm thick FePt films that exhibit similar behavior dictated by gradients in composition. Further, since the volume of ferromagnetically ordered spins changes with temperature in these structures, one can envision novel application in thermomagnetic sensors and switches.[12] For instance, symmetrically graded structure with the paramagnetic region in the center could show complex temperature dependent magnetic coupling, since the thickness of the paramagnetic interlayer region will be temperature dependent. In addition, rationally designed composition profiles could be employed to achieve specifically desired temperature and field dependencies. Such an approach could be used to tailor the magnetocaloric response of a medium to realize advances in applications such as magnetic refrigeration.[21, 22]

CONCLUSION

PNR measurements reveal the temperature and field dependent evolution of the second order phase transition in $Ni_{x(z)}Cu_{1-x(z)}$, a ferromagnet with a continuous gradient in exchange strength. The data are consistent with mean-field simulations of the system, and reveal a boundary between a weakly ordered (effectively paramagnetic) region and a more strongly ordered (effectively ferromagnetic) region. The position of this boundary is controllable by temperature, and the boundary moves continuously and reversibly within the structure. Application of a relatively modest 500 mT field is sufficient to significantly alter the magnetic profile between the magnetically disordered and more ordered states. Such temperature and field functionality, coupled with the relative ease of growth suggest this system could be of significant interest for a variety of novel thermomagnetic applications.

METHODS

Sample growth. Films were deposited using room temperature sputtering. The composition gradients were achieved by adjusting the deposition rates from two independent magnetron guns. Computer control allowed the net deposition rate to remain constant throughout the co-deposition process.

Polarized neutron reflectometry. PNR measurements were conducted on the PBR beamline at the NIST Center for Neutron Research. A wavelength 0.475 nm neutron beam was incident on the sample surface, and the specular reflectivity was measured as a function of wavevector transfer Q using a ^{3}He detector. H was applied in the plane of the sample, and an Fe/Si supermirror / Al-coil spin flipper assembly was used to polarize the incident neutron magnetic moment either parallel (+) or antiparallel (-) to H. A second supermirror/flipper array was used to analyze the spin state of the scattered beam (+ or -). The beam polarization was measured to be better than 96 % for all polarization states. Spin flip measurements were conducted at select conditions, and revealed no evidence of spin-flip scattering. The data were corrected for background (determined from measurements taken with the detector offset 0.3° from the specular condition), beam polarization, and beam footprint. Model fitting was done using the NIST Refl1D software package,[23] with parameter uncertainty determined using a Markov chain Monte Carlo algorithm.[24, 25]

CONTRIBUTIONS

C. W. and B. J. K. conceived and designed the experiments. H. F. B. grew samples. D. B. and H. F. B performed VSM measurements. D. B. and A. J. G. performed XRD measurements. A. J. G. performed SQUID measurements. B. J. K. performed and analyzed neutron measurements. P. A. K. wrote neutron modeling code. P. R. and A. B. were responsible for theory.

ACKNOWLEDGEMENTS

Work at RIT was supported by NSF-CAREER. Work at nanoGUNE was supported by the Spanish Government (Project No. MAT2012-36844).

* bkirby@nist.gov
† a.berger@nanogune.eu
‡ cwmsch@rit.edu

[1] C. A. Ramos, D. Lederman, A. R. King, and V. Jaccarino, Phys. Rev. Lett. **65**, 2913 (1990).
[2] R. W. Wang and D. L. Mills, Phys. Rev. B **46**, 11682 (1992).
[3] M. Marcellini, M. Parnaste, B. Hjorvarsson, and M. Wolff, Phys. Rev. B **79**, 14426 (2009).
[4] D. Suess, Appl. Phys. Lett. **89**, 113105 (2006).
[5] A. Berger, N. Supper, Y. Ikeda, B. Lengsfield, A. Moser, and E. E. Fullerton, Appl. Phys. Lett. **93**, 122502 (2008).
[6] A. Berger, E. Fullerton, H. Van Do, and N. Supper, "magnetic recording media comprising a coupling layer controlling the ferromagnetic coupling between a recording layer having coercivity and magnetic anisotropy and a layer comprising cobalt alloys; improved writeability," (2010), uS Patent 7,687,157.
[7] B. J. Kirby, J. E. Davies, K. Liu, S. M. Watson, G. T. Zimany, R. D. Shull, P. A. Kienzle, and J. A. Borchers, Phys. Rev. B **81**, 100405 (2010).

[8] B. J. Kirby, , P. K. Greene, B. B. Maranville, J. E. Davies, and K. Liu, J. Appl. Phys. **117**, 063905 (2015).

[9] C. L. Graët, T. R. Charlton, M. McLaren, M. Loving, S. A. Morley, C. J. Kinane, R. M. D. Brydson, L. H. Lewis, S. Langridge, and C. H. Marrows, APL Materials **3**, 041802 (2015).

[10] C. Kittel, in *Introduction to Solid State Physics* (John Wiley and Sons, 2005) Chap. 12, p. 325, 8th ed.

[11] S. A. Ahern, M. J. C. Martin, and W. A. Sucksmith, Proc. Roy. Soc. A **248**, 145 (1958).

[12] A. F. Kravets, A. Timoshevskii, B. Yanchitsky, M. A. Bergmann, J. Buhler, S. Andersson, and V. Korenivski, Phys. Rev. B **86**, 214413 (2012).

[13] The expected change in total magnetic moment corresponding to the x gradient is not accounted for in the simulation, but should not have a significant effect on the results.

[14] See supplementary material as [URL will be inserted by journal] for the explicit functional form.

[15] C. F. Majkrzak, K. V. O'Donovan, and N. F. Berk, in *Neutron Scattering from Magnetic Materials*, edited by T. Chatterji (Elsevier Science, New York, 2005).

[16] T. S. Santos, B. J. Kirby, S. Kumar, S. J. May, J. A. Borchers, B. B. Maranville, J. Zarestky, S. G. E. te Velthuis, J. van den Brink, and A. Bhattacharya, Phys. Rev. Lett. **107**, 167202 (2011).

[17] C. He, A. J. Grutter, M. Gu, N. D. Browning, Y. Takamura, B. J. Kirby, J. A. Borchers, J. W. Kim, M. R. Fitzsimmons, X. Zhai, V. V. Mehta, F. J. Wong, and Y. Suzuki, Phys. Rev. Lett. **109**, 197202 (2012).

[18] See supplementary material as [URL will be inserted by journal] for details of PNR model fitting.

[19] See supplementary material as [URL will be inserted by journal] for details of field cycling.

[20] See supplementary material as [URL will be inserted by journal] for comparison.

[21] K. G. Sandeman, Scripta Materialia **67**, 566 (2012).

[22] C. W. Miller, D. D. Belyea, and B. J. Kirby, Journal of Vacuum Science and Technology A **32**, 040802 (2014).

[23] B. J. Kirby, P. A. Kienzle, B. B. Maranville, N. F. Berk, J. Krycka, F. Heinrich, and C. F. Majkrzak, Curr. Opin. Colloid Interface Sci. **17**, 44 (2012).

[24] in *ISO/IEC Guide 98-3-:2008/Suppl 1:2008, Propagation of distributions using a Monte Carlo method* (International Organization for Standardization, Geneva, Switzerland, 2008) 1st ed.

[25] J. A. Vrugt, C. J. F. T. Braak, C. G. H. Diks, D. Higdon, B. A. Robinson, and J. M. Hyman, Int J Nonlinear Sci Numer Simul **10**, 273 (2009).

Supplementary Material for "Spatial evolution of the phase transition in compositionally graded magnetic films"

B. J. Kirby,[1,*] H. F. Belliveau,[2] D. D. Belyea,[2] T. Eggers,[2] P. A. Kienzle,[1] A. J. Grutter,[1] P. Riego,[3] A. Berger,[3,†] and Casey W. Miller[4,‡]

[1]*Center for Neutron Research, NIST, Gaithersburg, MD 20899, USA*

[2]*Department of Physics, University of South Florida, Tampa, FL 33620*

[3]*CIC nanoGUNE Consolider, E-20018 Donostia - San Sebastian, Spain*

[4]*School of Chemistry and Materials Science, Rochester Institute of Technology, Rochester, NY, 14623*

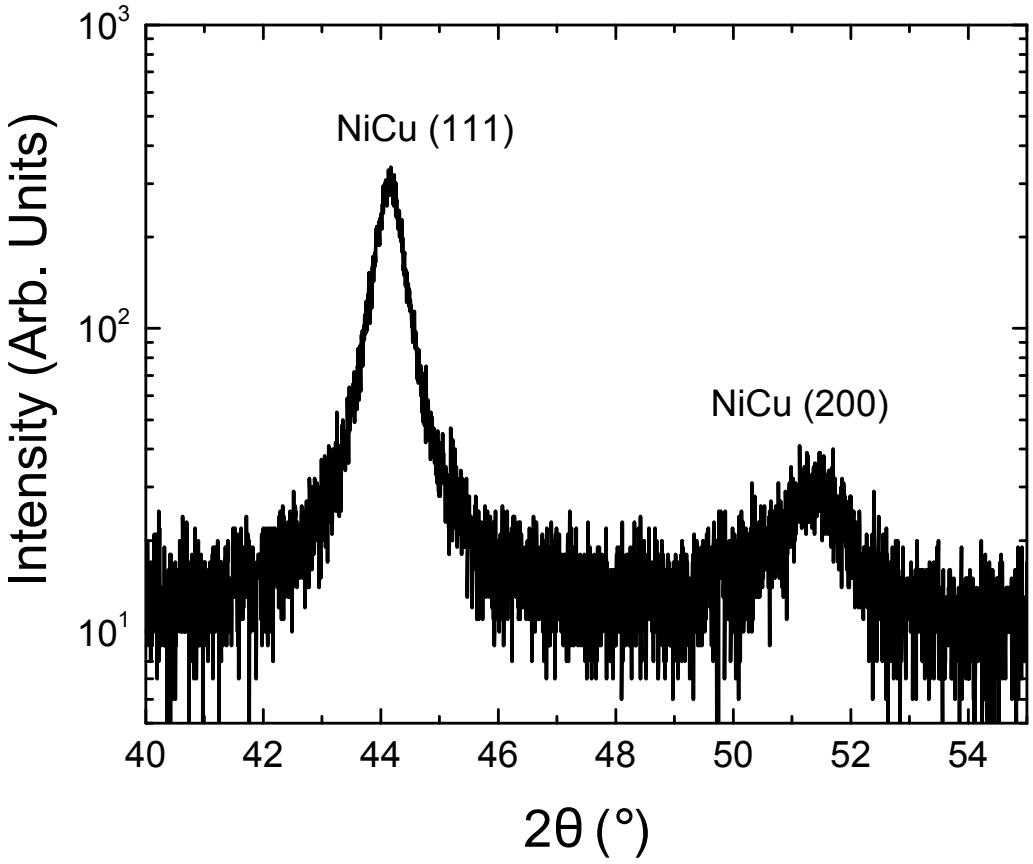

FIG. S1. XRD spectra for the graded Ni_xCu_{1-x} sample.

PRIMARY SAMPLE CHARACTERIZATION

X-ray diffraction (XRD) measurements of the graded Ni_xCu_{1-x} sample were performed using Cu-kα radiation (wavelength 0.154 nm), and are shown in Figure S1. A strong NiCu (111) peak is observed, along with a weaker NiCu (200), indicating a preferred (111) orientation. Magnetometry measurements of the graded Ni_xCu_{1-x} and the uniform $Ni_{0.70}Cu_{0.30}$ and $Ni_{0.61}Cu_{0.39}$ control samples are shown in Figure S2. Panel (a) shows the normalized temperature dependent magnetization for all three samples in a 500 mT field as measured with a vibrating sample magnetometer (VSM) (solid lines). The graded sample curve falls in between that of the control samples. Fig. S2(b) shows the temperature-dependent magnetization for the graded sample, as measured in a 5 mT field with a SQUID magnetometer (solid line). By integrating over the entire magnetization depth profile, the net magnetization as determined from PNR can be compared to that determined from VSM and SQUID. Such normalized integrals are shown as open circles in Fig. S2, and reveal excellent agree-

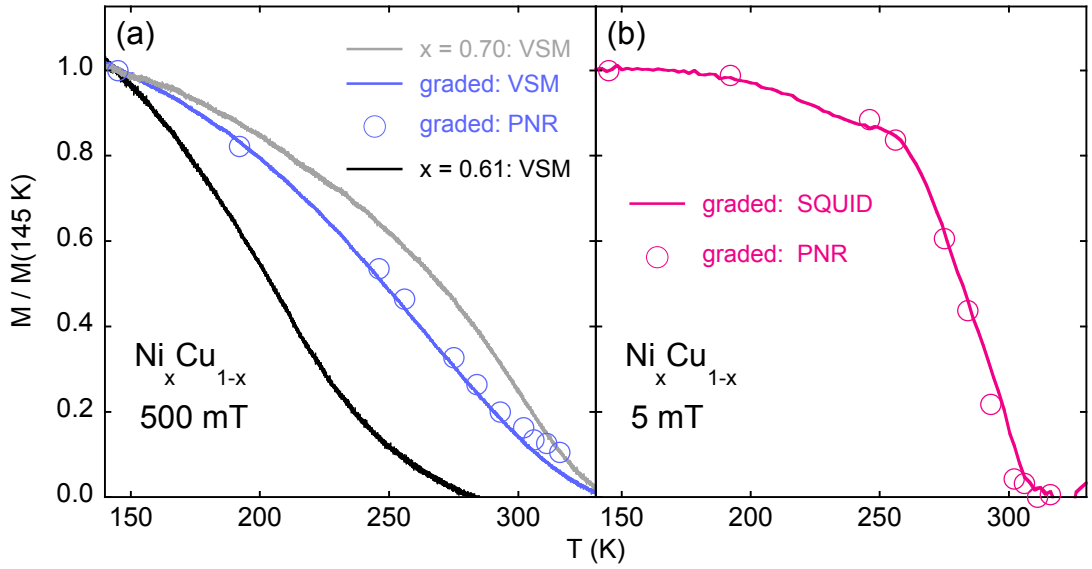

FIG. S2. (a) Normalized magnetizations for the uniform $x = 0.7$, graded $x = 0.61$ -0.70, and uniform $x = 0.61$ Ni_xCu_{1-x} samples in 500 mT. Lines correspond to VSM measurements, while the circles correspond to integrated magnetization profiles determined from PNR. (b) Normalized magnetization for the graded sample in 5 mT as determined from SQUID (lines) and PNR (open circles).

ment between the PNR and VSM (SQUID) results. This agreement strongly corroborates the validity of the PNR model fitting.

FIELD CYCLING AT 275 K

Figure 3 in the main text shows PNR spectra and model fits corresponding to three distinct conditions:

- I: 500 mT, 145 K, $T < T_C(x = 0.61) < T_C(x = 0.70)$,
  high field, below all nominal T_C
- II: 500 mT, 275 K, $T_C(x = 0.61) < T < T_C(x = 0.70)$,
  high field, between min and max nominal T_C
- III: 5 mT, 275 K, $T_C(x = 0.61) < T < T_C(x = 0.70)$,
  low field, between min and max nominal T_C

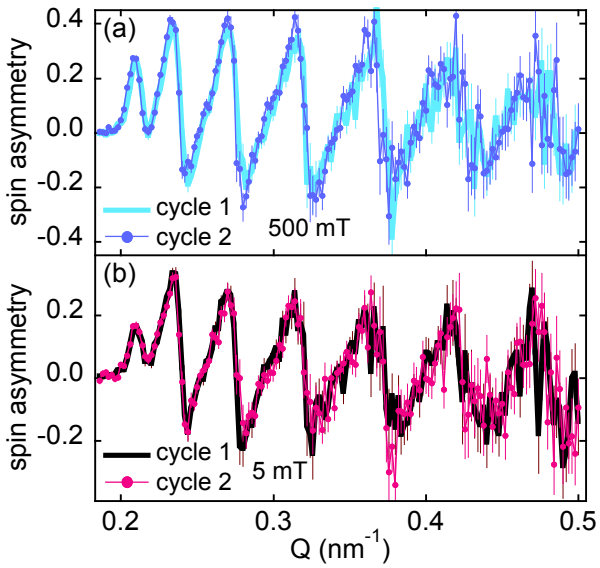

FIG. S3. Comparison of spin asymmetries measured in cycle 1 (dots) and cycle 2 (lines) in state II (a) and III (b). Error bars correspond to ± 1 standard deviation.

PNR measurements were taken for states II and III (cycle 1), the field was reduced to 5 mT, and measurements for state II and III were repeated (cycle 2). Figure S3 shows the measured cycle 1 and cycle 2 spin asymmetries for state II (panel a) and state III (panel b). The cycle 1 and cycle 2 spectra are essentially identical, demonstrating that the profile can be switched between the very different state II and III profiles (shown in Fig. 3 (d-e) in the main text) with application of a 500 mT field.

PNR MODEL FITTING

The depth (z) profiles of the the in-plane magnetization component parallel to the neutron spin axis (i.e. parallel to H), and the nuclear scattering length density $\rho = \sum_i N_i b_i$ (where N is the number density, b is the isotope specific nuclear scattering length, and the summation is over each type of isotope present in the material), can be determined through model fitting of $R^{++}(Q)$ and $R^{--}(Q)$.[1, 2]

Model fitting was done using the NIST Refl1D software package,[3] with parameter uncertainty determined using a Markov chain Monte Carlo algorithm.[4, 5] The nuclear profile of the sample is described in terms of an infinite Si backing media, a linearly graded Ni_xCu_{1-x} slab, a Ta capping layer, and an infinite vacuum incident media. For the Ni_xCu_{1-x} layer,

literature values are assumed for the scattering lengths of Ni (9.4 fm) and Cu (6.6 fm),[6] x is assumed to increase linearly from 0.61 - 0.70 with increasing distance from the substrate, and N is a fitted parameter assumed to be constant across the layer. The magnetic profile of Ni_xCu_{1-x} is described in terms of a closed form function that accurately reproduces the T and H dependent profiles determined from the mean field simulations described in the main text, convoluted with a sloped line (to account for the increase in total moment corresponding to the linear increase in x). Specifically, the magnetic profile is modeled in terms of three free parameters:

- z_C, critical depth: position of the weakly ordered / strongly ordered quasi phase boundary
- h, effective field: accounts for effects of the applied magnetic field,and also incorporates the effect of the interlayer exchange interaction along the T_C-gradient direction
- M_{max}, maximum magnetization: peak magnetization of the profile (acts as a scaling factor)

And constants:

- $A = \frac{dJ}{dz} = 3.2 \times 10^{-3}$ nm^{-1}, the slope of the depth dependent exchange coupling constant
- $x_i = 0.61$, Ni concentration near the Si substrate
- $x_f = 0.70$, Ni concentration near the Ta cap

The functional form is described,

$$\alpha = 3\left(h^2 - \frac{A(z-z_C)}{1+A(z-z_C)}\right),\ \beta = h(h^2-3),$$
$$\gamma = \frac{\beta^2}{4} + \frac{\alpha^3}{27},\ H_\pm = \frac{1}{2}\left(1 \pm \frac{\gamma}{|\pm\gamma|}\right),$$

$$\delta = \frac{\frac{-\beta}{2} + \sqrt{H_+\gamma}}{\left|\frac{-\beta}{2} + \sqrt{H_+\gamma}\right|}\left|\frac{-\beta}{2} + \sqrt{H_+\gamma}\right|^{\frac{1}{3}} + \frac{\frac{-\beta}{2} - \sqrt{H_+\gamma}}{\left|\frac{-\beta}{2} - \sqrt{H_+\gamma}\right|}\left|\frac{-\beta}{2} - \sqrt{H_+\gamma}\right|^{\frac{1}{3}},$$

$$\epsilon = 2\left(\frac{\beta^2}{4} - H_-\gamma\right)^{\frac{1}{6}} \cos\left(\frac{1}{3}\arctan\left[\frac{-2\sqrt{-H_-\gamma}}{\beta}\right]\right),$$

$$\zeta(z) = \frac{x_f - xi}{z_f - zi}z + x_i,$$

$$\eta(z) = \zeta(z)\tanh\left[(1 + A(z - z_C))\left(h + \delta H_+ + \epsilon H_-\right)\right],$$

$$M(z) = \eta(z)\frac{M_{max}}{\eta(z_f)}.$$

Thus, in the spirit of the mean-field simulation, the magnetization profiles determined from PNR are parameterized in terms of weakly and strongly ordered regions separated by a boundary at depth z_C. As with the mean-field simulation, we assume that z_C is field-independent, and that h is temperature-independent. Therefore, for the magnetic profiles, z_C was held constant for model fitting of data measured at constant T (within $\pm$ 1 K), and h was held constant for fitting of data measured at the same H. Values of h were determined by simultaneous fitting of data measured at [500 mT, 145 K], [5 mT, 145 K], [500 mT, 275 K], and [5 mT, 275 K]. Values of z_C were determined by simultaneously fitting data measured at the same temperature. In addition to fitting parameters corresponding to the nuclear and magnetic depth profiles, fitting parameters were employed to account for small measurement-to-measurement variations in intensity normalization and sample alignment with respect to the detector. These "nuisance" parameters were found to be effectively uncorrelated with parameters of interest.

It is important to address the choice of model in interpreting the PNR results. We have chosen a tightly constrained "exchange strength gradient" (ESG) model based on a thermodynamic mean-field simulation of the system that we believe provides the most insight into the underlying physics. However, in practice, the PNR data could also be well fit by alternate models that have some of the same basic features of the ESG model. To give an example of our sensitivity, Figure S4 shows model fitting results for data taken at 5 mT and 275 K, using three different models:

- "ESG": the exchange strength gradient model inspired by mean field simulations, as discussed in the main text

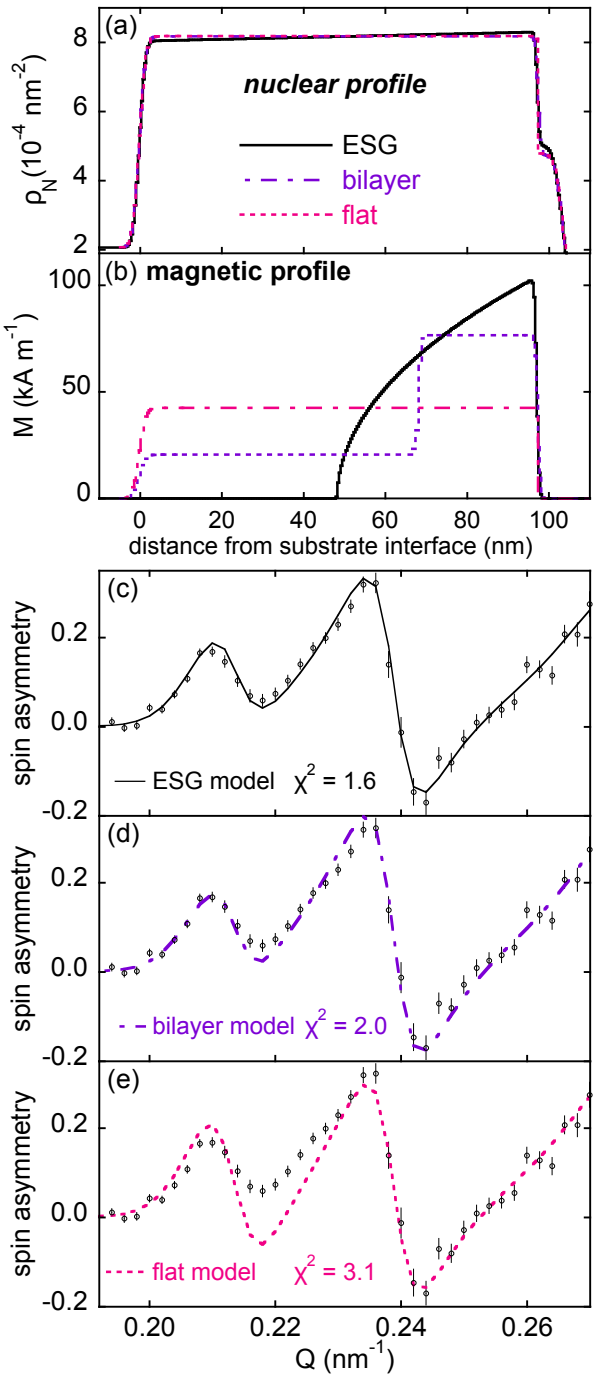

FIG. S4. Comparison of three different models used to fit data taken at 5 mT / 275 K. (a) Nuclear profiles. (b) Magnetization profiles. (c-e) Low Q fits to the data corresponding to the profiles in panels (a-b). Error bars correspond to ± 1 standard deviation.

- "bilayer": Ni_xCu_{1-x} has a uniform nuclear profile, but is divided into 2 sub-layers with different M

- "flat": Ni_xCu_{1-x} treated as uniform layer

The best-fit nuclear and magnetic profiles for each type of model are shown in Fig. S4(a) and (b) respectively, and the corresponding fits to the data are shown in (c-e). The fits are shown at low Q, and plotted as spin asymmetry to highlight the most statistically significant model-to-model variations. Normalized χ^2 goodness of fit values (corresponding to R^{++} and R^{--}, not the spin asymmetry) are shown in the insets. The ESG model (panel c) results in a good fit, clearly consistent with the data. Conversely, the flat model (e) clearly fails to reproduce the two lowest Q spin asymmetry peaks. However, adding a second magnetic layer, as in the bilayer model (d), results in a fit that reproduces the data nearly as well as the ESG model. The 1 standard deviation significance range associated with χ^2 is estimated to be less than 0.05 for all three models.[7] Thus, from a quantitative perspective, the ESG model produces a significantly better fit than the either the bilayer or flat models. This model comparison illustrates that these PNR measurements indeed provide sensitivity to the depth distribution of magnetization in the Ni_xCu_{1-x} film, but that the exact profiles and derived parameters are of course dependent on the model and boundary conditions chosen.

---

* bkirby@nist.gov

† a.berger@nanogune.eu

‡ cwmsch@rit.edu

[1] C. F. Majkrzak, K. V. O'Donovan, and N. F. Berk, in *Neutron Scattering from Magnetic Materials*, edited by T. Chatterji (Elsevier Science, New York, 2005).

[2] C. F. Majkrzak, Physica B **221**, 342 (1996).

[3] B. J. Kirby, P. A. Kienzle, B. B. Maranville, N. F. Berk, J. Krycka, F. Heinrich, and C. F. Majkrzak, Curr. Opin. Colloid Interface Sci. **17**, 44 (2012).

[4] in *ISO/IEC Guide 98-3-:2008/Suppl 1:2008, Propagation of distributions using a Monte Carlo method* (International Organization for Standardization, Geneva, Switzerland, 2008) 1st ed.

[5] J. A. Vrugt, C. J. F. T. Braak, C. G. H. Diks, D. Higdon, B. A. Robinson, and J. M. Hyman, Int J Nonlinear Sci Numer Simul **10**, 273 (2009).

[6] I. S. Anderson, P. J. Brown, J. M. Carpenter, G. Lander, R. Pynn, J. M. Rowe, O. Schrpf, V. F. Sears, and B. T. M. Willish, in *International Tables for Crystallography* (Wiley, Hoboken, New Jersey, New York, 2006) Chap. 4.4, p. 430.

[7] W. H. Press, S. A. Teukolsky, W. T. Vetterling, and B. P. Flannery, in *Numerical Recipes* (Cambridge University Press, 2007) Chap. 15, p. 807, 3rd ed.